

## Improved Measurement of the Electroweak Penguin

### Process $B \rightarrow X_s \ell^+ \ell^-$

K. Abe,<sup>10</sup> K. Abe,<sup>46</sup> N. Abe,<sup>49</sup> I. Adachi,<sup>10</sup> H. Aihara,<sup>48</sup> M. Akatsu,<sup>24</sup> Y. Asano,<sup>53</sup>  
T. Aso,<sup>52</sup> V. Aulchenko,<sup>2</sup> T. Aushev,<sup>14</sup> T. Aziz,<sup>44</sup> S. Bahinipati,<sup>6</sup> A. M. Bakich,<sup>43</sup>  
Y. Ban,<sup>36</sup> M. Barbero,<sup>9</sup> A. Bay,<sup>20</sup> I. Bedny,<sup>2</sup> U. Bitenc,<sup>15</sup> I. Bizjak,<sup>15</sup> S. Blyth,<sup>29</sup>  
A. Bondar,<sup>2</sup> A. Bozek,<sup>30</sup> M. Bračko,<sup>22,15</sup> J. Brodzicka,<sup>30</sup> T. E. Browder,<sup>9</sup> M.-C. Chang,<sup>29</sup>  
P. Chang,<sup>29</sup> Y. Chao,<sup>29</sup> A. Chen,<sup>26</sup> K.-F. Chen,<sup>29</sup> W. T. Chen,<sup>26</sup> B. G. Cheon,<sup>4</sup>  
R. Chistov,<sup>14</sup> S.-K. Choi,<sup>8</sup> Y. Choi,<sup>42</sup> Y. K. Choi,<sup>42</sup> A. Chuvikov,<sup>37</sup> S. Cole,<sup>43</sup>  
M. Danilov,<sup>14</sup> M. Dash,<sup>55</sup> L. Y. Dong,<sup>12</sup> R. Dowd,<sup>23</sup> J. Dragic,<sup>23</sup> A. Drutskoy,<sup>6</sup>  
S. Eidelman,<sup>2</sup> Y. Enari,<sup>24</sup> D. Epifanov,<sup>2</sup> C. W. Everton,<sup>23</sup> F. Fang,<sup>9</sup> S. Fratina,<sup>15</sup>  
H. Fujii,<sup>10</sup> N. Gabyshev,<sup>2</sup> A. Garmash,<sup>37</sup> T. Gershon,<sup>10</sup> A. Go,<sup>26</sup> G. Gokhroo,<sup>44</sup>  
B. Golob,<sup>21,15</sup> M. Grosse Perdekamp,<sup>38</sup> H. Guler,<sup>9</sup> J. Haba,<sup>10</sup> F. Handa,<sup>47</sup> K. Hara,<sup>10</sup>  
T. Hara,<sup>34</sup> N. C. Hastings,<sup>10</sup> K. Hasuko,<sup>38</sup> K. Hayasaka,<sup>24</sup> H. Hayashii,<sup>25</sup> M. Hazumi,<sup>10</sup>  
E. M. Heenan,<sup>23</sup> I. Higuchi,<sup>47</sup> T. Higuchi,<sup>10</sup> L. Hinz,<sup>20</sup> T. Hojo,<sup>34</sup> T. Hokuue,<sup>24</sup>  
Y. Hoshi,<sup>46</sup> K. Hoshina,<sup>51</sup> S. Hou,<sup>26</sup> W.-S. Hou,<sup>29</sup> Y. B. Hsiung,<sup>29</sup> H.-C. Huang,<sup>29</sup>  
T. Igaki,<sup>24</sup> Y. Igarashi,<sup>10</sup> T. Iijima,<sup>24</sup> A. Imoto,<sup>25</sup> K. Inami,<sup>24</sup> A. Ishikawa,<sup>10</sup> H. Ishino,<sup>49</sup>  
K. Itoh,<sup>48</sup> R. Itoh,<sup>10</sup> M. Iwamoto,<sup>3</sup> M. Iwasaki,<sup>48</sup> Y. Iwasaki,<sup>10</sup> R. Kagan,<sup>14</sup> H. Kakuno,<sup>48</sup>  
J. H. Kang,<sup>56</sup> J. S. Kang,<sup>17</sup> P. Kapusta,<sup>30</sup> S. U. Kataoka,<sup>25</sup> N. Katayama,<sup>10</sup> H. Kawai,<sup>3</sup>  
H. Kawai,<sup>48</sup> Y. Kawakami,<sup>24</sup> N. Kawamura,<sup>1</sup> T. Kawasaki,<sup>32</sup> N. Kent,<sup>9</sup> H. R. Khan,<sup>49</sup>  
A. Kibayashi,<sup>49</sup> H. Kichimi,<sup>10</sup> H. J. Kim,<sup>19</sup> H. O. Kim,<sup>42</sup> Hyunwoo Kim,<sup>17</sup> J. H. Kim,<sup>42</sup>  
S. K. Kim,<sup>41</sup> T. H. Kim,<sup>56</sup> K. Kinoshita,<sup>6</sup> P. Koppenburg,<sup>10</sup> S. Korpar,<sup>22,15</sup> P. Krizan,<sup>21,15</sup>  
P. Krokovny,<sup>2</sup> R. Kulasiri,<sup>6</sup> C. C. Kuo,<sup>26</sup> H. Kurashiro,<sup>49</sup> E. Kurihara,<sup>3</sup> A. Kusaka,<sup>48</sup>

A. Kuzmin,<sup>2</sup> Y.-J. Kwon,<sup>56</sup> J. S. Lange,<sup>7</sup> G. Leder,<sup>13</sup> S. E. Lee,<sup>41</sup> S. H. Lee,<sup>41</sup>  
 Y.-J. Lee,<sup>29</sup> T. Lesiak,<sup>30</sup> J. Li,<sup>40</sup> A. Limosani,<sup>23</sup> S.-W. Lin,<sup>29</sup> D. Liventsev,<sup>14</sup>  
 J. MacNaughton,<sup>13</sup> G. Majumder,<sup>44</sup> F. Mandl,<sup>13</sup> D. Marlow,<sup>37</sup> T. Matsuishi,<sup>24</sup>  
 H. Matsumoto,<sup>32</sup> S. Matsumoto,<sup>5</sup> T. Matsumoto,<sup>50</sup> A. Matyja,<sup>30</sup> Y. Mikami,<sup>47</sup>  
 W. Mitaroff,<sup>13</sup> K. Miyabayashi,<sup>25</sup> Y. Miyabayashi,<sup>24</sup> H. Miyake,<sup>34</sup> H. Miyata,<sup>32</sup> R. Mizuk,<sup>14</sup>  
 D. Mohapatra,<sup>55</sup> G. R. Moloney,<sup>23</sup> G. F. Moorhead,<sup>23</sup> T. Mori,<sup>49</sup> A. Murakami,<sup>39</sup>  
 T. Nagamine,<sup>47</sup> Y. Nagasaka,<sup>11</sup> T. Nakadaira,<sup>48</sup> I. Nakamura,<sup>10</sup> E. Nakano,<sup>33</sup> M. Nakao,<sup>10</sup>  
 H. Nakazawa,<sup>10</sup> Z. Natkaniec,<sup>30</sup> K. Neichi,<sup>46</sup> S. Nishida,<sup>10</sup> O. Nitoh,<sup>51</sup> S. Noguchi,<sup>25</sup>  
 T. Nozaki,<sup>10</sup> A. Ogawa,<sup>38</sup> S. Ogawa,<sup>45</sup> T. Ohshima,<sup>24</sup> T. Okabe,<sup>24</sup> S. Okuno,<sup>16</sup>  
 S. L. Olsen,<sup>9</sup> Y. Onuki,<sup>32</sup> W. Ostrowicz,<sup>30</sup> H. Ozaki,<sup>10</sup> P. Pakhlov,<sup>14</sup> H. Palka,<sup>30</sup>  
 C. W. Park,<sup>42</sup> H. Park,<sup>19</sup> K. S. Park,<sup>42</sup> N. Parslow,<sup>43</sup> L. S. Peak,<sup>43</sup> M. Pernicka,<sup>13</sup>  
 J.-P. Perroud,<sup>20</sup> M. Peters,<sup>9</sup> L. E. Piilonen,<sup>55</sup> A. Poluektov,<sup>2</sup> F. J. Ronga,<sup>10</sup> N. Root,<sup>2</sup>  
 M. Rozanska,<sup>30</sup> H. Sagawa,<sup>10</sup> M. Saigo,<sup>47</sup> S. Saitoh,<sup>10</sup> Y. Sakai,<sup>10</sup> H. Sakamoto,<sup>18</sup>  
 T. R. Sarangi,<sup>10</sup> M. Satapathy,<sup>54</sup> N. Sato,<sup>24</sup> O. Schneider,<sup>20</sup> J. Schümann,<sup>29</sup> C. Schwanda,<sup>13</sup>  
 A. J. Schwartz,<sup>6</sup> T. Seki,<sup>50</sup> S. Semenov,<sup>14</sup> K. Senyo,<sup>24</sup> Y. Settai,<sup>5</sup> R. Seuster,<sup>9</sup>  
 M. E. Sevier,<sup>23</sup> T. Shibata,<sup>32</sup> H. Shibuya,<sup>45</sup> B. Shwartz,<sup>2</sup> V. Sidorov,<sup>2</sup> V. Siegle,<sup>38</sup>  
 J. B. Singh,<sup>35</sup> A. Somov,<sup>6</sup> N. Soni,<sup>35</sup> R. Stamen,<sup>10</sup> S. Stanič,<sup>53,\*</sup> M. Starič,<sup>15</sup> A. Sugi,<sup>24</sup>  
 A. Sugiyama,<sup>39</sup> K. Sumisawa,<sup>34</sup> T. Sumiyoshi,<sup>50</sup> S. Suzuki,<sup>39</sup> S. Y. Suzuki,<sup>10</sup> O. Tajima,<sup>10</sup>  
 F. Takasaki,<sup>10</sup> K. Tamai,<sup>10</sup> N. Tamura,<sup>32</sup> K. Tanabe,<sup>48</sup> M. Tanaka,<sup>10</sup> G. N. Taylor,<sup>23</sup>  
 Y. Teramoto,<sup>33</sup> X. C. Tian,<sup>36</sup> S. Tokuda,<sup>24</sup> S. N. Tovey,<sup>23</sup> K. Trabelsi,<sup>9</sup> T. Tsuboyama,<sup>10</sup>  
 T. Tsukamoto,<sup>10</sup> K. Uchida,<sup>9</sup> S. Uehara,<sup>10</sup> T. Uglov,<sup>14</sup> K. Ueno,<sup>29</sup> Y. Unno,<sup>3</sup> S. Uno,<sup>10</sup>  
 Y. Ushiroda,<sup>10</sup> G. Varner,<sup>9</sup> K. E. Varvell,<sup>43</sup> S. Villa,<sup>20</sup> C. C. Wang,<sup>29</sup> C. H. Wang,<sup>28</sup>  
 J. G. Wang,<sup>55</sup> M.-Z. Wang,<sup>29</sup> M. Watanabe,<sup>32</sup> Y. Watanabe,<sup>49</sup> L. Widhalm,<sup>13</sup>  
 Q. L. Xie,<sup>12</sup> B. D. Yabsley,<sup>55</sup> A. Yamaguchi,<sup>47</sup> H. Yamamoto,<sup>47</sup> S. Yamamoto,<sup>50</sup>  
 T. Yamanaka,<sup>34</sup> Y. Yamashita,<sup>31</sup> M. Yamauchi,<sup>10</sup> Heyoung Yang,<sup>41</sup> P. Yeh,<sup>29</sup> J. Ying,<sup>36</sup>  
 K. Yoshida,<sup>24</sup> Y. Yuan,<sup>12</sup> Y. Yusa,<sup>47</sup> H. Yuta,<sup>1</sup> S. L. Zang,<sup>12</sup> C. C. Zhang,<sup>12</sup> J. Zhang,<sup>10</sup>  
 L. M. Zhang,<sup>40</sup> Z. P. Zhang,<sup>40</sup> V. Zhilich,<sup>2</sup> T. Ziegler,<sup>37</sup> D. Žontar,<sup>21,15</sup> and D. Zürcher<sup>20</sup>

(The Belle Collaboration)

<sup>1</sup>*Aomori University, Aomori*

<sup>2</sup>*Budker Institute of Nuclear Physics, Novosibirsk*

- <sup>3</sup>*Chiba University, Chiba*
- <sup>4</sup>*Chonnam National University, Kwangju*
- <sup>5</sup>*Chuo University, Tokyo*
- <sup>6</sup>*University of Cincinnati, Cincinnati, Ohio 45221*
- <sup>7</sup>*University of Frankfurt, Frankfurt*
- <sup>8</sup>*Gyeongsang National University, Chinju*
- <sup>9</sup>*University of Hawaii, Honolulu, Hawaii 96822*
- <sup>10</sup>*High Energy Accelerator Research Organization (KEK), Tsukuba*
- <sup>11</sup>*Hiroshima Institute of Technology, Hiroshima*
- <sup>12</sup>*Institute of High Energy Physics,  
Chinese Academy of Sciences, Beijing*
- <sup>13</sup>*Institute of High Energy Physics, Vienna*
- <sup>14</sup>*Institute for Theoretical and Experimental Physics, Moscow*
- <sup>15</sup>*J. Stefan Institute, Ljubljana*
- <sup>16</sup>*Kanagawa University, Yokohama*
- <sup>17</sup>*Korea University, Seoul*
- <sup>18</sup>*Kyoto University, Kyoto*
- <sup>19</sup>*Kyungpook National University, Taegu*
- <sup>20</sup>*Swiss Federal Institute of Technology of Lausanne, EPFL, Lausanne*
- <sup>21</sup>*University of Ljubljana, Ljubljana*
- <sup>22</sup>*University of Maribor, Maribor*
- <sup>23</sup>*University of Melbourne, Victoria*
- <sup>24</sup>*Nagoya University, Nagoya*
- <sup>25</sup>*Nara Women's University, Nara*
- <sup>26</sup>*National Central University, Chung-li*
- <sup>27</sup>*National Kaohsiung Normal University, Kaohsiung*
- <sup>28</sup>*National United University, Miao Li*
- <sup>29</sup>*Department of Physics, National Taiwan University, Taipei*
- <sup>30</sup>*H. Niewodniczanski Institute of Nuclear Physics, Krakow*
- <sup>31</sup>*Nihon Dental College, Niigata*
- <sup>32</sup>*Niigata University, Niigata*
- <sup>33</sup>*Osaka City University, Osaka*

- <sup>34</sup>*Osaka University, Osaka*
- <sup>35</sup>*Panjab University, Chandigarh*
- <sup>36</sup>*Peking University, Beijing*
- <sup>37</sup>*Princeton University, Princeton, New Jersey 08545*
- <sup>38</sup>*RIKEN BNL Research Center, Upton, New York 11973*
- <sup>39</sup>*Saga University, Saga*
- <sup>40</sup>*University of Science and Technology of China, Hefei*
- <sup>41</sup>*Seoul National University, Seoul*
- <sup>42</sup>*Sungkyunkwan University, Suwon*
- <sup>43</sup>*University of Sydney, Sydney NSW*
- <sup>44</sup>*Tata Institute of Fundamental Research, Bombay*
- <sup>45</sup>*Toho University, Funabashi*
- <sup>46</sup>*Tohoku Gakuin University, Tagajo*
- <sup>47</sup>*Tohoku University, Sendai*
- <sup>48</sup>*Department of Physics, University of Tokyo, Tokyo*
- <sup>49</sup>*Tokyo Institute of Technology, Tokyo*
- <sup>50</sup>*Tokyo Metropolitan University, Tokyo*
- <sup>51</sup>*Tokyo University of Agriculture and Technology, Tokyo*
- <sup>52</sup>*Toyama National College of Maritime Technology, Toyama*
- <sup>53</sup>*University of Tsukuba, Tsukuba*
- <sup>54</sup>*Utkal University, Bhubaneswer*
- <sup>55</sup>*Virginia Polytechnic Institute and State University, Blacksburg, Virginia 24061*
- <sup>56</sup>*Yonsei University, Seoul*

(Dated: November 5, 2018)

## Abstract

We present an improved measurement of the branching fraction for the electroweak penguin process  $B \rightarrow X_s \ell^+ \ell^-$ , where  $\ell$  is an electron or a muon and  $X_s$  is a hadronic system containing an  $s$ -quark. The measurement is based on a sample of  $152 \times 10^6$   $\Upsilon(4S) \rightarrow B\bar{B}$  events collected with the Belle detector at the KEKB  $e^+e^-$  asymmetric-energy collider. The  $X_s$  hadronic system is reconstructed from one  $K^\pm$  or  $K_s^0$  and up to four pions, where at most one pion can be neutral. Summing over both lepton flavors, the inclusive branching fraction is measured to be  $\mathcal{B}(B \rightarrow X_s \ell^+ \ell^-) = (4.11 \pm 0.83(\text{stat})_{-0.70}^{+0.74}(\text{syst})) \times 10^{-6}$  for  $m(\ell^+ \ell^-) > 0.2 \text{ GeV}/c^2$ .

PACS numbers: 13.20.He, 12.15.Ji, 14.65.Fy, 14.40.Nd

## INTRODUCTION

In the Standard Model (SM), the rare decay  $B \rightarrow X_s \ell^+ \ell^-$  proceeds through a  $b \rightarrow s \ell^+ \ell^-$  transition, which is forbidden at tree level. Such a flavor-changing neutral current (FCNC) process can occur at higher order via electroweak penguin and  $W^+ W^-$  box diagrams. The  $b \rightarrow s \ell^+ \ell^-$  transition therefore allows deeper insight into the effective Hamiltonian that describes FCNC processes and is sensitive to the effects of non-SM physics that may enter these loops; see, for example, Refs. [1, 2].

Recent SM calculations of the inclusive  $B \rightarrow X_s \ell^+ \ell^-$  branching fractions predict  $\mathcal{B}(B \rightarrow X_s e^+ e^-) = (6.9 \pm 1.0) \times 10^{-6}$  [ $(4.2 \pm 0.7) \times 10^{-6}$  for  $m(\ell^+ \ell^-) > 0.2 \text{ GeV}/c^2$ ] and  $\mathcal{B}(B \rightarrow X_s \mu^+ \mu^-) = (4.2 \pm 0.7) \times 10^{-6}$  [1, 3]. Both the Belle and BaBar Collaborations have observed exclusive  $B \rightarrow K \ell^+ \ell^-$  and  $K^* \ell^+ \ell^-$  decays [4, 5, 6, 7] and have measured inclusive  $B \rightarrow X_s \ell^+ \ell^-$  decay [8, 9].

In this analysis, we study the inclusive  $B \rightarrow X_s \ell^+ \ell^-$  process by semi-inclusively reconstructing the final state from a pair of electrons or muons and a hadronic system consisting of one  $K^\pm$  or  $K_s^0$  and up to four pions, where at most one pion can be neutral. This semi-inclusive-reconstruction approach [10] allows approximately 53% of the full inclusive rate to be reconstructed. If the fraction of modes containing a  $K_L^0$  is taken to be equal to that containing a  $K_S^0$ , the missing states that remain unaccounted for represent  $\sim 30\%$  of the total rate. We require the hadronic mass for the selected final states to be less than  $2.0 \text{ GeV}/c^2$  to reduce combinatorial background. We correct for the missing modes and the effect of the hadronic mass cut to extract the inclusive  $B \rightarrow X_s \ell^+ \ell^-$  decay rate for  $m(\ell^+ \ell^-) > 0.2 \text{ GeV}/c^2$ .

The measurement of inclusive  $B \rightarrow X_s \ell^+ \ell^-$  decay in this paper updates and supersedes our previous publication[8] described above, which was based on a sample of  $65 \times 10^6$   $B\bar{B}$  pairs. The measurement reported here is currently the most precise.

## THE BELLE DETECTOR AND DATA SAMPLE

We use a data sample collected on the  $\Upsilon(4S)$  resonance with the Belle detector at the KEKB  $e^+ e^-$  asymmetric-energy collider (3.5 GeV on 8 GeV) [11]. This sample comprises  $152 \times 10^6$   $B$  meson pairs, corresponding to an integrated luminosity of  $140.0 \text{ fb}^{-1}$ . A detailed

description of the Belle detector can be found elsewhere [12]. A three-layer silicon vertex detector (SVD) and a 50-layer central drift chamber (CDC) are used for tracking and particle identification for charged particles. An array of aerogel threshold Čerenkov counters (ACC) and time-of-flight scintillation counters (TOF) are used for the charged particle identification. An electromagnetic calorimeter comprised of Tl-doped CsI crystals (ECL) measures the energy of electromagnetic particles and is also used for electron identification. These detectors are located inside a superconducting solenoid coil that provides a 1.5 T magnetic field. An iron flux-return located outside of the coil is instrumented with resistive plate counters to identify muons (KLM).

Particle identification for the final state particles  $e^\pm$ ,  $\mu^\pm$ ,  $K^\pm$ ,  $K_s^0$ ,  $\pi^\pm$  and  $\pi^0$  is important for this analysis. Electron identification is based on the ratio of the cluster energy to the track momentum ( $E/p$ ), the specific energy-loss measurement ( $dE/dx$ ) with the CDC, the position and shower shape of the cluster in the ECL and the response from the ACC. Muon identification is based on the hit positions and the depth of penetration into the ECL and KLM. Electrons and muons are required to have lab-frame momenta greater than 0.4 GeV/ $c$  and 0.8 GeV/ $c$ , respectively. For the muon identification, we also apply a kaon veto to select good muon candidates. Bremsstrahlung photons from electrons are recovered by combining an electron with photons within a small angular region around the electron direction. Charged kaon candidates are selected by using information from the ACC, TOF and CDC. The kaon selection efficiency is 90% with a pion to kaon mis-identification probability of 6%. After selecting the electron, muon and charged kaon candidate tracks, the remaining charged particles are assumed to be charged pions.  $K_s^0$  candidates are reconstructed from pairs of oppositely-charged tracks with  $|m(\pi^+\pi^-) - m(K_s^0)| < 15 \text{ MeV}/c^2$ . We impose additional  $K_s^0$  selection criteria based on the distance and the direction of the  $K_s^0$  vertex and the impact parameters of the daughter tracks. We require the charged tracks except for those used in the  $K_s^0$  reconstruction to have impact parameters with respect to the nominal interaction point of less than 1.0 cm in the radial direction and 5.0 cm along the beam direction. Neutral pions are required to have lab-frame energy greater than 400 MeV, photon daughter energies greater than 50 MeV, and a  $\gamma\gamma$  invariant mass that satisfies  $|m(\gamma\gamma) - m(\pi^0)| < 10 \text{ MeV}/c^2$ .

## ANALYSIS OVERVIEW

In this analysis, we reconstruct the inclusive  $B \rightarrow X_s \ell^+ \ell^-$  decays with a semi-inclusive-reconstruction technique from a pair of electrons or muons and one of 18 reconstructed hadronic states. Here the hadronic system consists of one  $K^\pm$  or  $K_s^0$  and up to four pions (at most one pion can be neutral). Compared to a fully inclusive approach, this method has the advantage of having strong kinematical discrimination against background by using the beam-energy constrained mass  $M_{bc} = \sqrt{E_{beam}^2 - p_B^2}$  and the energy difference  $\Delta E = E_B - E_{beam}$ , where  $E_{beam}$  is the beam energy and  $E_B$  ( $p_B$ ) is the reconstructed  $B$  meson energy (3-momentum). All quantities are evaluated in the  $e^+e^-$  center-of-mass system (CM).

In addition to the discrimination, further background suppression to reduce the large combinatorial backgrounds is necessary. The main contribution to the combinatorial background comes from semileptonic decays in  $B\bar{B}$  events. In these events,  $B \rightarrow X_s \ell^+ \ell^-$  candidates are reconstructed with the decay products from both  $B\bar{B}$  mesons. This background has a significant amount of missing energy due to the neutrinos from the semileptonic decays. Another contribution to the combinatorial background comes from continuum events, which are effectively suppressed with event-shape variables.

There are two background sources that can peak in  $M_{bc}$  and  $\Delta E$ . The first comes from  $B \rightarrow J/\psi X$  and  $B \rightarrow \psi(2S)X$  decays with  $J/\psi(\psi(2S)) \rightarrow \ell^+ \ell^-$ . This peaking background is efficiently removed with cuts on the dilepton mass  $m(\ell^+ \ell^-)$ . The resulting veto sample provides a large control sample of decays with a signature identical to that of the signal. The second comes from  $B \rightarrow K^\pm(K_s^0)n\pi$  ( $n > 1$ ) decays with misidentification of two charged pions as leptons. We estimate these peaking background contaminations, then subtract them from the signal yield.

For the  $B \rightarrow X_s \ell^+ \ell^-$  event simulation, we use EVTGEN [13] for the event generator, JETSET [14] to hadronize the system consisting of a strange quark and a spectator quark, and GEANT [15] for the detector simulation. In the event generation,  $B \rightarrow X_s \ell^+ \ell^-$  events are produced with a combination of exclusive and inclusive models. In the hadronic mass region of  $m(X_s) < 1.1 \text{ GeV}/c^2$ , exclusive  $B \rightarrow K^{(*)} \ell^+ \ell^-$  decays are generated according to Refs. [1, 16], where the relevant form factors are computed using light-cone QCD sum rules. In the region  $m(X_s) > 1.1 \text{ GeV}/c^2$ , event generation is based on a non-resonant model following Refs. [1, 17] and the Fermi motion model of Ref. [18].



## EVENT SELECTION

Events are required to have a well determined primary vertex, be tagged as multi-hadron events, and contain two electrons (muons) having lab-frame momenta greater than 0.4 GeV/ $c$  for electrons and 0.8 GeV/ $c$  for muons. Dilepton candidates are selected for  $e^+e^-$  or  $\mu^+\mu^-$  pairs. Both leptons are required to originate from the same vertex and satisfy the requirement  $|\Delta z| < 0.015$  cm. Here,  $\Delta z$  is the distance between the two leptons along the beam direction; the  $z$ -coordinate of each lepton is determined at the point of closest approach to the beam axis.

Charmonium backgrounds are reduced by removing  $B$  candidates with a dilepton mass in the ranges  $-0.40 \text{ GeV}/c^2 < M_{ee(\gamma)} - M_{J/\psi} < 0.15 \text{ GeV}/c^2$ ,  $-0.25 \text{ GeV}/c^2 < M_{\mu\mu} - M_{J/\psi} < 0.10 \text{ GeV}/c^2$ ,  $-0.25 \text{ GeV}/c^2 < M_{ee(\gamma)} - M_{\psi(2S)} < 0.10 \text{ GeV}/c^2$ , and  $-0.15 \text{ GeV}/c^2 < M_{\mu\mu} - M_{\psi(2S)} < 0.10 \text{ GeV}/c^2$ . If one of the electrons from a  $J/\psi$  or  $\psi(2S)$  decay erroneously picks up a random photon in the Bremsstrahlung-recovery process, the dilepton mass can increase sufficiently to evade the above cuts. Therefore the charmonium veto is applied to the dilepton mass before and after Bremsstrahlung recovery. Using the simulation, we estimate the remaining peaking charmonium background to be  $1.20 \pm 0.28$  events and  $1.33 \pm 0.21$  events for  $e^+e^-$  modes and  $\mu^+\mu^-$  modes, respectively.

The potential peaking background from  $B \rightarrow X_s \gamma$  decays, followed by conversion of the photon into an  $e^+e^-$  pair in the detector material, and  $\pi^0$  Dalitz decay is a concern for the  $e^+e^-$  modes only. We remove this background by requiring  $m(e^+e^-) > 0.2 \text{ GeV}/c^2$ .

Using the  $\ell^+\ell^-$  pair,  $B \rightarrow X_s \ell^+\ell^-$  candidates are formed by adding either a  $K^\pm$  or a  $K_s^0$  and up to four pions, but no more than one  $\pi^0$ . In this manner, eighteen different hadronic topologies are considered:  $K^\pm$ ,  $K^\pm\pi^0$ ,  $K^\pm\pi^\mp$ ,  $K^\pm\pi^\mp\pi^0$ ,  $K^\pm\pi^\mp\pi^\pm$ ,  $K^\pm\pi^\mp\pi^\pm\pi^0$ ,  $K^\pm\pi^\mp\pi^\pm\pi^\mp$ ,  $K^\pm\pi^\mp\pi^\pm\pi^\mp\pi^0$ ,  $K^\pm\pi^\mp\pi^\pm\pi^\mp\pi^\pm$ ,  $K_s^0$ ,  $K_s^0\pi^0$ ,  $K_s^0\pi^\pm$ ,  $K_s^0\pi^\pm\pi^0$ ,  $K_s^0\pi^\mp\pi^\pm$ ,  $K_s^0\pi^\mp\pi^\pm\pi^0$ ,  $K_s^0\pi^\mp\pi^\pm\pi^\mp$ ,  $K_s^0\pi^\mp\pi^\pm\pi^\mp\pi^0$ , and  $K_s^0\pi^\mp\pi^\pm\pi^\mp\pi^\pm$ .

After forming the  $B \rightarrow X_s \ell^+\ell^-$  candidates, we carry out the background suppression. The largest background sources are random combinations of dileptons with a kaon and pions that originate from continuum  $q\bar{q}$  ( $q = u, d, s, c$ ) production or from semileptonic  $B$  decays. We reject the  $q\bar{q}$  background with a Fisher discriminant [19] ( $\mathcal{F}_{\text{SFW}}$ ) based on a modified set of Fox-Wolfram moments [20] that differentiate the event topology, by applying a cut  $\mathcal{F}_{\text{SFW}} > -1.0$ . In the semileptonic  $B$  decay background, both  $B$  mesons

decay into leptons or two leptons are produced from the  $b \rightarrow c \rightarrow s, d$  decay chain. We combine the missing mass ( $M_{\text{miss}}$ ) and the total visible energy ( $E_{\text{vis}}$ ) into another Fisher discriminant ( $\mathcal{F}_{\text{miss}}$ ) to reject the  $B$  decay background. The missing mass is defined as  $M_{\text{miss}} = \sqrt{(2E_{\text{beam}} - \sum E_i)^2 - |\sum \vec{p}_i|^2}$ , where  $E_{\text{beam}}$  is the CM beam energy and  $E_i$  ( $\vec{p}_i$ ) is the reconstructed energy (3-momentum) for the charged particle or the photon in the CM frame. The sum runs over all the charged particles with a pion mass hypothesis and all photons. The total visible energy is also calculated using the charged particles and photons. We require the selection cut of  $\mathcal{F}_{\text{miss}} > 1.2$ .

We further reduce the background using  $\Delta E$  and  $\chi_{B\text{vtx}}^2$  with the selection criteria:  $-0.10 \text{ GeV}/c < \Delta E < 0.05 \text{ GeV}/c$  for the electron mode ( $-0.05 \text{ GeV}/c < \Delta E < 0.05 \text{ GeV}/c$  for the muon mode), and  $\chi_{B\text{vtx}}^2/NDF < 10.0$ . Here,  $\chi_{B\text{vtx}}^2$  is the fitted chi squared of the  $B$  vertex constructed from the charged daughter particles except for the  $K_S^0$  daughter tracks. We reject candidates with the  $X_s$  invariant mass greater than  $2.0 \text{ GeV}/c^2$ . This condition removes a large fraction of the combinatorial background while retaining 99% of the signal.

At this stage, there is an average of 1.6  $B$  candidates per event in the signal simulation. We retain only the  $B$  candidate with the largest signal likelihood. We select the following six variables as the background-discrimination variables, and calculate the likelihood functions based on the distributions of the variables:  $\Delta E$ ,  $\Delta E^{\text{ROE}}$ ,  $\chi_{B\text{vtx}}^2$ ,  $\cos \theta_B$ ,  $\mathcal{F}_{\text{SFW}}$ , and  $\mathcal{F}_{\text{miss}}$ . The energy difference  $\Delta E^{\text{ROE}}$  is formed by combining all charged tracks and neutral calorimeter clusters not included in the  $B$  candidate, and  $\cos \theta_B$  is the cosine of the  $B$  flight direction with respect to the  $e^-$  beam direction in the CM frame.

The signal probability density functions (PDFs) are determined by applying fits to each distribution for signal MC events. For  $\Delta E$  and  $\chi_{B\text{vtx}}^2$ , we use the real charmonium-veto-event distributions to determine the PDFs, because we observe some discrepancy between the signal MC and the real charmonium-veto events. In the charmonium-veto-event distributions, we subtract the background shapes obtained by the  $M_{bc}$  side-band region. The normalization of the subtracted background events is determined by the number of background events in the  $M_{bc}$  signal region, which is estimated by fitting to the  $M_{bc}$  distribution with a Gaussian (signal) and an ARGUS [21] (BG) function. For  $\Delta E$ , we use distinct PDFs for the electron and muon modes. For the background PDFs, we use background MC events.

The variables  $\Delta E$ ,  $\Delta E^{\text{ROE}}$ , and  $\mathcal{F}_{\text{miss}}$  are effective at rejecting  $B\bar{B}$  background, especially

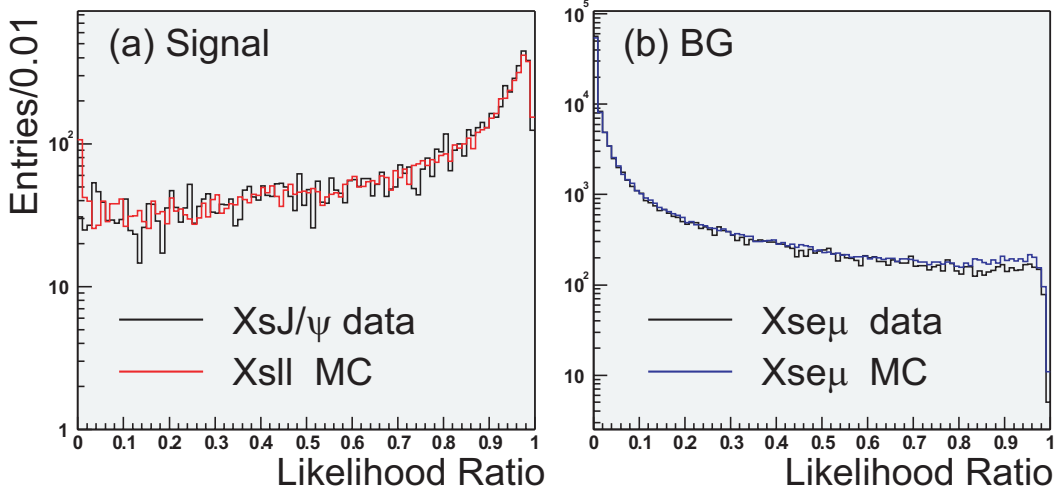


FIG. 1: The likelihood ratios for (a) signal and (b) background events. The red (blue) and black histograms in the signal (background) likelihood distributions show signal MC (MC  $B \rightarrow X_s e^\pm \mu^\mp$  events) and the real charmonium veto sample (real  $B \rightarrow X_s e^\pm \mu^\mp$  events), respectively.

for events with two semileptonic decays, which have large missing energy. For continuum suppression, the event-shape variable  $\mathcal{F}_{\text{SFW}}$  and  $\cos\theta_B$  are useful.  $\chi_{Bvtx}^2$  is effective to reject the random combinatorial background in the high multiplicity modes.

We then calculate the likelihoods  $\mathcal{L}_{S,B} = \prod_{i=1}^6 p_{S,B}^i$  where  $p_{S,B}^i$  are the PDFs for the background-discrimination variable  $i$  for the signal ( $S$ ) and the background ( $B$ ), respectively. Then we obtain the final discriminating variable, the likelihood ratio  $\mathcal{R} = \mathcal{L}_S / (\mathcal{L}_S + \mathcal{L}_B)$ . Only the  $B$  candidate with the largest  $\mathcal{R}$  value is retained. We find that the correct candidate is reconstructed in 84% of the events.

In order to check the obtained likelihood ratio, we compare the real charmonium-veto events and signal MC for the signal likelihood ratio, and the real and background MC  $B \rightarrow X_s e^\pm \mu^\mp$  events that are selected using the nominal selection criteria but requiring that the two leptons have different flavor, for the background likelihood ratio. Figures 1(a) and (b) show the likelihood ratios for the signal and background events, respectively. We observe good agreement in both figures.

The final suppression of the combinatorial background is achieved with the likelihood ratio  $\mathcal{R}$ . Using the simulation, the cut on  $\mathcal{R}$  is optimized to maximize the statistical significance of the signal. This optimization is performed in the two  $m(X_s)$  regions  $m(X_s) < 1.1 \text{ GeV}/c^2$ ,

and  $1.1 \text{ GeV}/c^2 < m(X_s) < 2.0 \text{ GeV}/c^2$ , resulting in the cuts  $\mathcal{R} > 0.3$  and  $0.9$ .

After applying all selection criteria, a sample of 155  $B \rightarrow X_s e^+ e^-$  and 112  $B \rightarrow X_s \mu^+ \mu^-$  candidates remains in the signal  $M_{bc}$  region. Here we define the signal  $M_{bc}$  region as  $5.27 \text{ GeV}/c^2 < M_{bc} < 5.29 \text{ GeV}/c^2$ . According to the simulation, the background remaining at this stage of the analysis consists mostly of  $B\bar{B}$  events (80% and 72% of the total background in the electron and muon channels, respectively). Using the signal MC simulation, the probability to select the correctly reconstructed candidate is estimated to be 91%.

## MAXIMUM LIKELIHOOD FIT

We perform an extended, unbinned maximum likelihood fit to the  $M_{bc}$  distribution in the region  $M_{bc} > 5.2 \text{ GeV}/c^2$  to extract the signal yield as well as the shape and yield of the combinatorial background. The likelihood function  $\mathcal{L}$  is expressed as:

$$\mathcal{L} = \frac{e^{-(N_{sig} + N_{peak} + N_{total\_BG})}}{N!} \prod_{i=1}^N [(N_{sig} + N_{peak}) \mathcal{P}_i^{sig} + \sum_{BG} N_{BG} \mathcal{P}_i^{BG}]$$

$$N_{total\_BG} = N_{pc} + N_{cf} + N_{comb}$$

$$\sum_{BG} N_{BG} \mathcal{P}_i^{BG} = N_{pc} \mathcal{P}_i^{pc} + N_{cf} \mathcal{P}_i^{cf} + N_{comb} \mathcal{P}_i^{comb}$$

where  $N$  and  $i$  denote the total number and index of candidate events, respectively.  $N_{sig}$ ,  $N_{peak}$ ,  $N_{pc}$ ,  $N_{cf}$ , and  $N_{comb}$  represent the yields of the signal, peaking background, combinatorial background from peaking background, cross-feed events from the mis-reconstructed  $B \rightarrow X_s \ell^+ \ell^-$  decays, and combinatorial background, respectively.  $\mathcal{P}_i^{sig}$  is the signal PDF. We use the same PDF for signal and peaking background events.  $\mathcal{P}_i^{pc}$ ,  $\mathcal{P}_i^{cf}$ , and  $\mathcal{P}_i^{comb}$  are the background component PDFs for combinatorial background from peaking background, cross feed, and combinatorial background, respectively.

The signal PDF  $\mathcal{P}_i^{sig}$  is described by a Gaussian for  $\mu^+ \mu^-$  modes as well as for  $e^+ e^-$  modes, since the Bremsstrahlung recovery and selection procedure for  $e^+ e^-$  modes lead to a negligible radiative tail in the  $M_{bc}$  distribution. The Gaussian shape parameters, the mean and the resolution  $\sigma$  values are determined from fits to the sum of a Gaussian and an ARGUS function for the real charmonium-veto data sample. The fits results in a signal  $M_{bc}$  mean and resolution, respectively, of  $m_{sig} = 5279.31 \pm 0.05 \text{ MeV}/c^2$  and  $\sigma_{sig} = 2.62 \pm 0.04 \text{ MeV}/c^2$  for the  $e^+ e^-$  modes, and  $m_{sig} = 5279.03 \pm 0.04 \text{ MeV}/c^2$  and  $\sigma_{sig} = 2.53 \pm 0.04 \text{ MeV}/c^2$  for

the  $\mu^+\mu^-$  modes. In the simulation, the Gaussian fit results for the  $M_{bc}$  distributions for correctly reconstructed signal are in agreement with the shape parameters extracted from the fits to the charmonium-veto sample. The signal yield  $N_{sig}$  is a free parameter in the likelihood fit.

The charmonium peaking background is estimated from the simulation to be  $1.20 \pm 0.28$  events in the electron modes and  $1.33 \pm 0.21$  events in the muon modes. The charmonium peaking background PDF is the same as that for signal since the signal PDF is extracted from the charmonium-veto data sample.

The size and shape of the hadronic peaking  $B\bar{B}$  background component arising from  $B \rightarrow D^{(*)}n\pi$  ( $n > 0$ ) decays with misidentification of two charged pions as leptons are derived directly from the real data by performing the analysis without the lepton identification requirements. By fitting the  $M_{bc}$  distribution to the sum of Gaussian and ARGUS functions, we get the mean and the resolution of  $m_{peak} = 5279.16 \pm 0.04$  MeV/ $c^2$  and  $\sigma_{peak} = 2.60 \pm 0.02$  MeV/ $c^2$ . Taking the  $\pi$  to  $\ell$  misidentification rates into account, the remaining hadronic peaking background is estimated to be  $N_{h-peak} = 0.03 \pm 0.001$  events for the  $e^+e^-$  modes and  $N_{h-peak} = 1.78 \pm 0.05$  events for the  $\mu^+\mu^-$  modes. Here we use the momentum and polar-angle dependent misidentification rate. The average misidentification rates for electrons and muons are 0.08% and 0.92%, respectively. In the likelihood fit, we also use the same signal PDF for the hadronic peaking-background PDF, because the fitted Gaussian shape-parameter values are consistent with those of the charmonium-veto data sample, and  $N_{peak}$  is fixed to the estimated values. Figures 2(a) and (b) show the  $M_{bc}$  distributions for the MC charmonium events for the electron and muon modes, and (c) and (d) show the  $M_{bc}$  distributions for real  $B \rightarrow X_s h^+ h^-$  events for the electron and muon modes, respectively.

The background component PDFs,  $\mathcal{P}_i^{pc}$ ,  $\mathcal{P}_i^{cf}$ , and  $\mathcal{P}_i^{comb}$  are given by an ARGUS shape. They describe the combinatorial contribution from peaking background events, from cross feed events, and from continuum events and  $B\bar{B}$  events, respectively. The ARGUS cutoff is determined by the beam energy in the  $\Upsilon(4S)$  rest frame,  $E_{beam} = 5.290$  GeV. The values of the ARGUS shape parameter for each background component are determined from the peaking background  $M_{bc}$  distribution shown in Fig.2 ( $\mathcal{P}_i^{pc}$ ), from incorrectly reconstructed signal MC events ( $\mathcal{P}_i^{cf}$ ), and from the fit to the real  $B \rightarrow X_s e^\pm \mu^\mp$  events selected using the nominal selection criteria but requiring that the two leptons have different flavor ( $\mathcal{P}_i^{comb}$ ). We fix the three ARGUS shape parameters,  $N_{pc}$ , and  $N_{cf}$ . The yield  $N_{comb}$  is taken as a

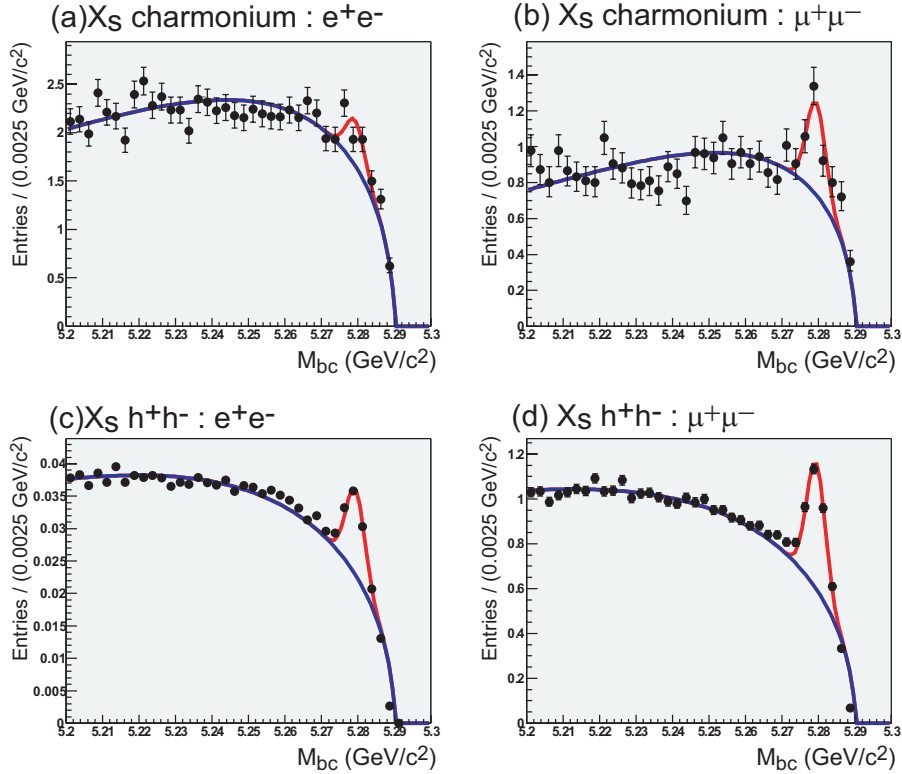


FIG. 2:  $M_{bc}$  distributions for MC charmonium events for (a) electron and (b) muon modes, and real  $B \rightarrow X_s h^+ h^-$  events for (c) electron and (d) muon modes.

free parameter in the likelihood fit.

## RESULTS

Using the fit parameterizations described above, we fit the  $M_{bc}$  distributions for the selected  $B \rightarrow X_s e^+ e^-$  and  $B \rightarrow X_s \mu^+ \mu^-$  candidates separately and obtain the results shown in Figure 3. The fit results are summarized in Table I. The statistical significance is  $\mathcal{S} = \sqrt{2(\ln \mathcal{L}_{max} - \ln \mathcal{L}_{max}^0)}$ , where  $\mathcal{L}_{max}$  represents the maximum likelihood for the fit and  $\mathcal{L}_{max}^0$  denotes the maximum likelihood for a different fit when the signal yield is fixed at  $N_{sig} = 0$ . The  $B \rightarrow X_s \ell^+ \ell^-$  signal yield presented in Table I is the sum of the  $B \rightarrow X_s e^+ e^-$  and  $B \rightarrow X_s \mu^+ \mu^-$  signal yields. A separate fit to the combined electron and muon channels gives a comparable result. Figure 3(d) shows the  $M_{bc}$  distribution for  $B \rightarrow X_s e^\pm \mu^\mp$  candidates. Applying the ARGUS fit to the  $M_{bc}$  distribution, there is no evidence for a

peaking background as expected.

Figures 4(a) and (b) show the distributions for the hadronic mass  $M_{X_s}$  and  $q^2 \equiv M_{\ell^+\ell^-}^2$  for the electron and muon channels combined, but they are obtained by performing the nominal likelihood fit in separate  $M_{X_s}$  and  $q^2$  regions. Figure 4(a) indicates that the observed signal includes contributions from final states across a range of hadronic masses, including hadronic systems with a mass above that of the  $K^*(892)$ .

The branching fraction  $\mathcal{B}$  for the signal is calculated from

$$\mathcal{B} = \frac{N_{sig}}{2N_{B\bar{B}} \epsilon}, \quad (1)$$

where  $N_{B\bar{B}} = (152.0 \pm 0.7) \times 10^6$  is the number of  $B\bar{B}$  pairs produced in  $140.0 \text{ fb}^{-1}$  and  $\epsilon$  is the signal efficiency.

## SYSTEMATIC UNCERTAINTIES

Systematic uncertainties are of two different types: those that affect the extraction of the number of signal events and those that affect the calculation of the branching fraction. The systematic uncertainties are summarized in Table II.

Uncertainties affecting the extraction of the signal yield are evaluated by varying the signal Gaussian parameters (mean and width) and the background shape parameter within  $\pm 1\sigma$  of the measured values from the charmonium veto data (signal) and the real  $B \rightarrow X_s e^\pm \mu^\mp$  events (background).

We estimate the uncertainties in the peaking-background shape and cross-feed events by comparing the signal yields obtained with and without the corresponding PDFs in the unbinned maximum likelihood fit to  $M_{bc}$ .

TABLE I: Results of the fit to the data: number of the signal candidates in the signal box, obtained signal yield, peaking backgrounds (fixed in the fit), and statistical significance.

Mode	Candidates	$N_{sig}$	$N_{peak}$	Signif.
$X_s e^+ e^-$	155	$31.8 \pm 10.2$	$1.24 \pm 0.28$	3.6
$X_s \mu^+ \mu^-$	112	$36.3 \pm 9.3$	$3.11 \pm 0.22$	4.7
$X_s \ell^+ \ell^-$	267	$68.4 \pm 13.8$	$4.35 \pm 0.36$	5.8

TABLE II: Summary of fractional systematic uncertainties (in %). The uncertainties in extracting the signal are presented first and those related to the signal efficiency and  $B\bar{B}$  counting are presented second.

Source	$X_s e^+e^-$	$X_s \mu^+\mu^-$
Signal shape	$\pm 1.4$	$\pm 0.5$
BG shape	$\pm 7.8$	$\pm 4.7$
Peaking background statistics	$\pm 0.9$	$\pm 0.6$
Peaking background shape	$\pm 4.3$	$\pm 2.1$
Cross-feed events	$\pm 4.1$	$\pm 2.2$
Signal yield total	$\pm 9.9$	$\pm 5.7$
Tracking efficiency	$\pm 3.5$	$\pm 3.5$
Lepton identification efficiency	$\pm 1.0$	$\pm 2.4$
Kaon identification efficiency	$\pm 0.8$	$\pm 0.8$
$\pi^\pm$ identification efficiency	$\pm 0.6$	$\pm 0.5$
$K_S^0$ efficiency	$\pm 0.7$	$\pm 0.8$
$\pi^0$ efficiency	$\pm 0.3$	$\pm 0.3$
$\mathcal{R}$ cut efficiency	$\pm 5.4$	$\pm 1.5$
Detector model subtotal	$\pm 6.6$	$\pm 4.7$
Fermi motion model	$+6.5$ $-2.4$	$+6.1$ $-2.3$
$\mathcal{B}(B \rightarrow K\ell^+\ell^-)$	$\pm 6.4$	$\pm 6.8$
$\mathcal{B}(B \rightarrow K^*\ell^+\ell^-)$	$\pm 7.0$	$\pm 7.8$
$K^*-X_s$ transition	$\pm 4.5$	$\pm 4.7$
Hadronization	$\pm 8.5$	$\pm 8.2$
Missing modes	$\pm 4.5$	$\pm 4.4$
Signal model subtotal	$+15.6$ $-14.4$	$+15.9$ $-14.9$
Monte Carlo statistics	$\pm 1.6$	$\pm 1.5$
$B\bar{B}$ counting	$\pm 0.5$	$\pm 0.5$
Efficiency and $N_{B\bar{B}}$ total	$+17.0$ $-15.9$	$+16.6$ $-15.7$
Total	$+19.7$ $-18.8$	$+17.6$ $-16.7$



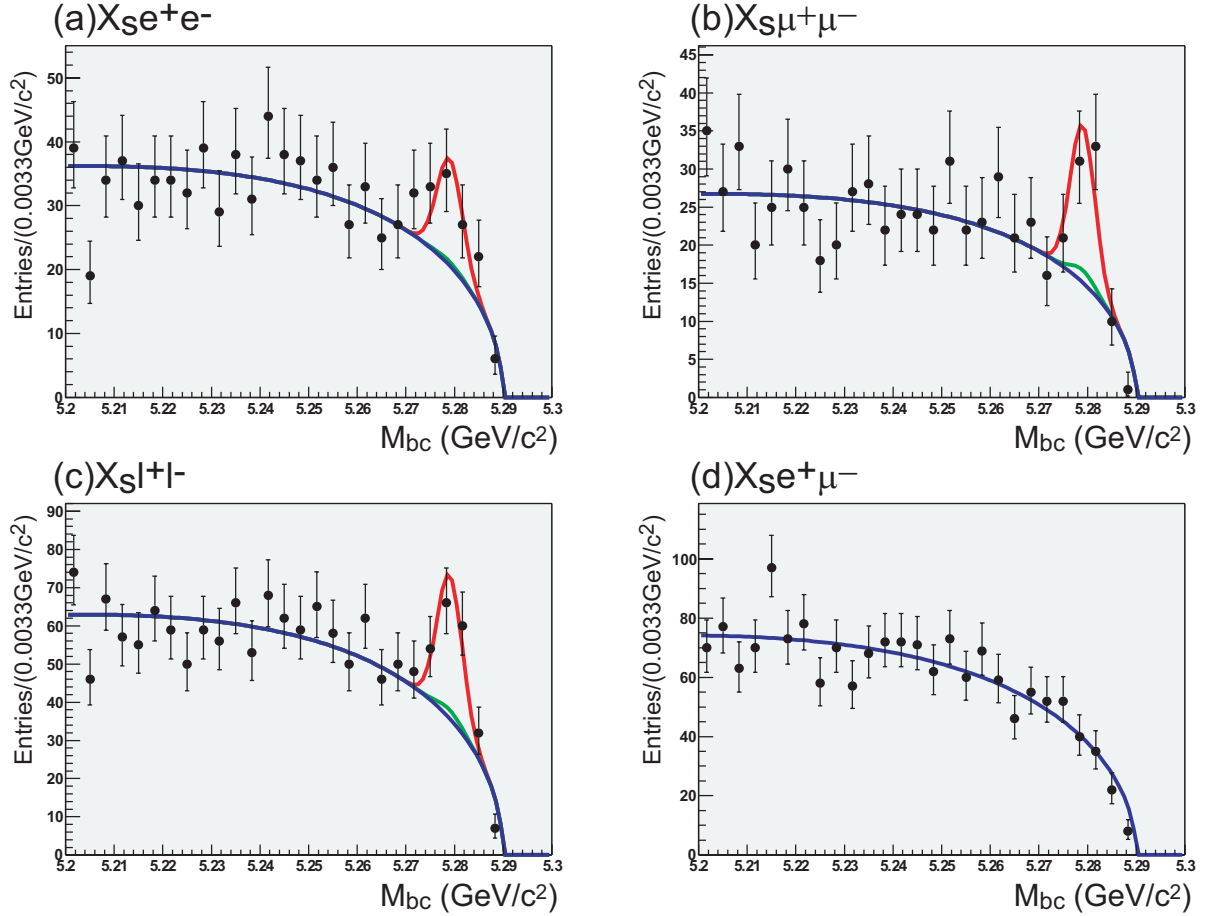


FIG. 3: Distributions of  $M_{bc}$  for selected (a)  $B \rightarrow X_s e^+ e^-$ , (b)  $B \rightarrow X_s \mu^+ \mu^-$ , (c)  $B \rightarrow X_s \ell^+ \ell^-$  ( $\ell = e, \mu$ ), and (d)  $B \rightarrow X_s e^\pm \mu^\mp$  candidates. The red lines represent the result of the fits, and the green and blue lines represent the peaking and combinatorial background components under the signal peaks, respectively.

Uncertainties affecting the signal efficiency originate from the detector modeling, from the simulation of signal decays, and from the estimate of the number of  $B$  mesons in the sample. By far the largest component is that due to the simulation of signal decays, discussed in detail below.

The detector modeling uncertainty is sensitive to the following uncertainties determined from the data: the uncertainty in the tracking efficiency of 1.0% per track; the uncertainty in the charged-particle identification efficiency of 0.5% per electron, 1.2% per muon, 1.0% per kaon and 0.8% per pion; and the uncertainty in the reconstruction efficiency of 4.5% per  $K_S^0$  and 3.3% per  $\pi^0$ . The efficiency of the likelihood ratio cut, which suppresses combinatorial

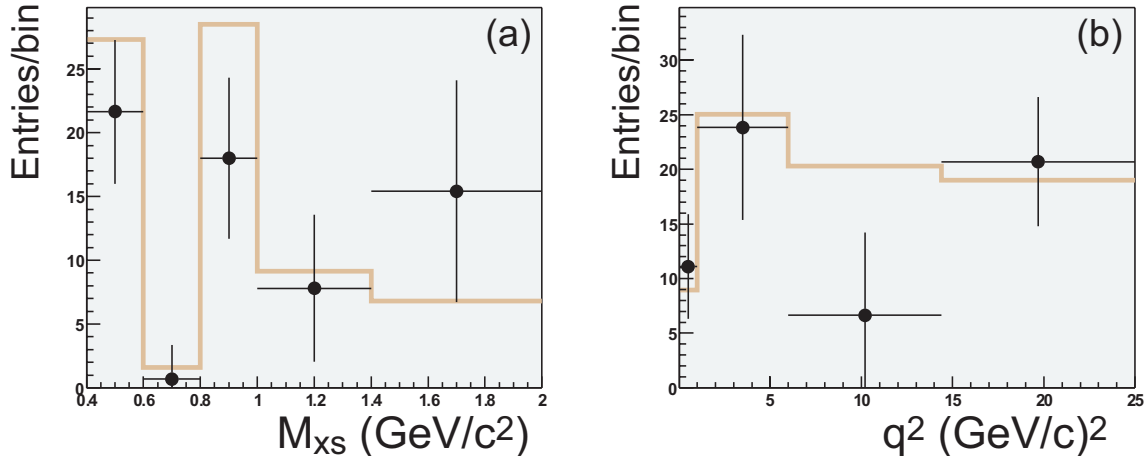


FIG. 4: Distributions of number of signal events as a function of (a) hadronic mass  $M_{X_s}$  and (b)  $q^2 \equiv M_{\ell^+\ell^-}^2$  for electron and muon channels combined for data (points) and Monte Carlo signal (histogram). The vertical error bars represent statistical errors only.

background, is checked with the charmonium-veto sample and the level of discrepancy with the simulation is taken as the corresponding uncertainty.

The dominant source of uncertainty arises from modeling the signal decays. Parameters of the Fermi motion model are varied in accordance with measurements of hadronic moments in semileptonic  $B$  decays [22] and the photon spectrum in inclusive  $B \rightarrow X_s \gamma$  decays [23]. The fractions of exclusive  $B \rightarrow K\ell^+\ell^-$  and  $B \rightarrow K^*\ell^+\ell^-$  decays are varied according to experimental [6, 7] and theoretical uncertainties [1], respectively. The transition point in  $m(X_s)$  between pure  $K^*\ell^+\ell^-$  and non-resonant  $X_s\ell^+\ell^-$  final states is varied by  $\pm 0.1 \text{ GeV}/c^2$ .

The non-resonant Monte Carlo event generator relies on JETSET to fragment and hadronize the system consisting of a final state  $s$  quark and a spectator quark from the  $B$  meson. Since the signal efficiencies depend strongly on the particle content of the final state, uncertainties in the number of charged and neutral pions and in the number of charged and neutral kaons translate into a significant uncertainty in the signal efficiency (for  $m(X_s) > 1.1 \text{ GeV}/c^2$ ).

The ratio between the generator yield for decay modes containing a  $K_s^0$  and that for modes containing a charged kaon is varied according to  $0.50 \pm 0.11$ , to allow for isospin violation in the decay chain. The ratio between the generator yield for decay modes containing one  $\pi^0$  meson and that for modes containing none is varied according to  $1.0 \pm 0.22$ . Uncertainties in

the ratios are set by the level of discrepancy between  $B \rightarrow J/\psi X$  real data and  $B \rightarrow X_s \ell^+ \ell^-$  Monte Carlo event sample.

The 18 modes selected in this analysis only capture about 53% of the full set of final states. Approximately 60% of the missing modes are due to final states with a  $K_L^0$  meson and their contribution can be determined from the  $K_S^0$  modes. However, we need to account for the uncertainty in the fraction of modes with too many pions or kaons (two extra kaons may be produced via  $s\bar{s}$  popping), as well as for modes with photons that do not originate from  $\pi^0$  decays but rather from  $\eta$ ,  $\eta'$ , etc. For final states with  $m(X_s) > 1.1 \text{ GeV}/c^2$ , we vary these fractions by  $\pm 5\%$  per  $\pi^0$ ,  $\pm 20\%$  for  $\eta$ ,  $\pm 30\%$  for  $N_\pi > 5$ , and  $\pm 50\%$  for  $\eta'$  and others.

Including systematic uncertainties, the measured branching fractions for  $m(\ell^+ \ell^-) > 0.2 \text{ GeV}/c^2$  are

$$\mathcal{B}(B \rightarrow X_s e^+ e^-) = (4.04 \pm 1.30_{-0.76}^{+0.80}) \times 10^{-6}, \quad (2)$$

$$\mathcal{B}(B \rightarrow X_s \mu^+ \mu^-) = (4.13 \pm 1.05_{-0.69}^{+0.73}) \times 10^{-6}, \quad (3)$$

$$\mathcal{B}(B \rightarrow X_s \ell^+ \ell^-) = (4.11 \pm 0.83_{-0.70}^{+0.74}) \times 10^{-6}, \quad (4)$$

where the first error is statistical and the second error is systematic. The combined  $B \rightarrow X_s \ell^+ \ell^-$  branching fraction is the weighted average of the branching fractions for the electron and muon channels, where we assume the individual branching fractions to be equal for  $m(\ell^+ \ell^-) > 0.2 \text{ GeV}/c^2$ . Table III summarizes the results of the analysis and lists both the statistical and systematic errors in the signal yields, the signal efficiencies and the branching fractions.

The branching fractions for each  $M_{X_s}$  and  $q^2$  bin are also measured, and summarized in Table IV. Figures 5(a) and (b) show the distributions of the differential branching fractions as a function of (a) hadronic mass  $M_{X_s}$  and (b)  $q^2 \equiv M_{\ell^+ \ell^-}^2$  for electron and muon channels combined.

## SUMMARY

Using a sample of  $152 \times 10^6 \Upsilon(4S) \rightarrow B\bar{B}$  events, we measure the branching fraction for the rare decay  $B \rightarrow X_s \ell^+ \ell^-$ , where  $\ell = e$  or  $\mu$  and  $X_s$  is a hadronic system is semi-inclusively reconstructed using 18 different hadronic states (with up to four pions). For

TABLE III: Summary of results: signal yield ( $N_{sig}$ ), statistical significance (Signif.), efficiency ( $\epsilon$ ) and branching fraction ( $\mathcal{B}$ ). In the case of the signal yield and the branching fraction, the first error is statistical and the second error is systematic. In the case of the signal efficiency, the first error corresponds to uncertainties in detector modeling,  $B\bar{B}$  counting, and Monte Carlo statistics, whereas the second error corresponds to the uncertainties in the signal model.

Mode	$N_{sig}$	Signif.	$\epsilon$ (%)	$\mathcal{B}$ ( $\times 10^{-6}$ )
$X_s e^+e^-$	$31.8 \pm 10.2 \pm 3.1$	3.6	$2.59 \pm 0.18$	$4.04 \pm 1.30$
$X_s \mu^+\mu^-$	$36.3 \pm 9.3 \pm 2.1$	4.7	$2.89 \pm 0.14$	$4.13 \pm 1.05$
$X_s \ell^+\ell^-$	$68.4 \pm 13.8 \pm 5.0$	5.8	$2.74 \pm 0.13$	$4.11 \pm 0.83$

TABLE IV: Branching fractions ( $\mathcal{B}$ ) for each bin of  $M_{X_s}$  and  $q^2$ . The first and second errors are statistical and systematic, respectively.

bin	$\mathcal{B}$ ( $\times 10^{-7}$ )	bin	$\mathcal{B}$ ( $\times 10^{-7}$ )
$M_{X_s}$ (GeV/ $c^2$ )		$q^2$ (GeV/ $c$ ) <sup>2</sup>	
[0.4, 0.6]	$3.75 \pm 0.96$	[0.04, 1.0]	$11.34 \pm 4.83$
[0.6, 0.8]	$0.36 \pm 0.88$	[1.0, 6.0]	$14.93 \pm 5.04$
[0.8, 1.0]	$6.65 \pm 2.25$	[6.0, 14.4]	$7.32 \pm 6.14$
[1.0, 1.4]	$10.50 \pm 6.90$	[14.4, 25.0]	$4.18 \pm 1.17$
[1.4, 2.0]	$46.59 \pm 23.37$		

$m(\ell^+\ell^-) > 0.2$  GeV/ $c^2$ , we observe a signal of  $68.4 \pm 13.8(stat) \pm 5.0(syst)$  events and obtain a branching fraction of

$$\mathcal{B}(B \rightarrow X_s \ell^+ \ell^-) = (4.11 \pm 0.83(stat)_{-0.70}^{+0.74}(syst)) \times 10^{-6},$$

with a statistical significance of  $5.8 \sigma$ .

This result is consistent with the recent prediction by Ali *et al.* [1], our previous inclusive  $B \rightarrow X_s \ell^+ \ell^-$  measurement [8], and that of the BaBar collaboration [9], within errors.

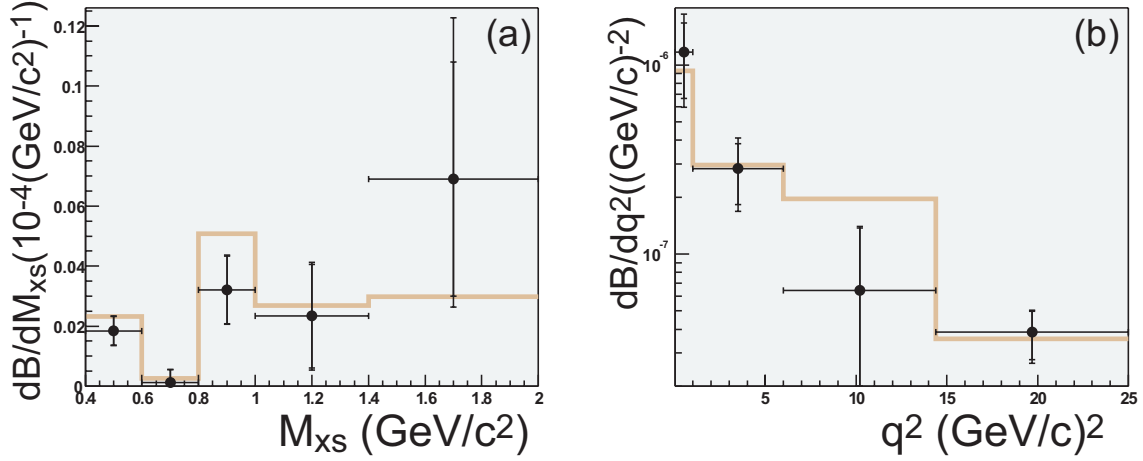


FIG. 5: Differential branching fraction as a function of (a) hadronic mass  $M_{X_s}$  and (b)  $q^2 \equiv M_{\ell^+\ell^-}^2$  for electron and muon channels combined for data (points) and Monte Carlo signal (histogram). The outer (inner) error bars represent the total (statistical) errors.

### Acknowledgments

The authors wish to thank Gudrun Hiller, Tobias Hurth and Gino Ishidori for their helpful suggestions. We have also benefited from suggestions by Stephane Willocq regarding event generation with EVTGEN. We are grateful for the KEKB accelerator group for their excellent operation of the KEKB accelerator. We acknowledge support from the Ministry of Education, Culture, Sports, Science, and Technology of Japan and the Japan Society for the Promotion of Science; the Australian Research Council and the Australian Department of Industry, Science and Resources; the National Science Foundation of China under contract No. 10175071; the Department of Science and Technology of India; the BK21 program of the Ministry of Education of Korea and the CHEP SRC program of the Korea Science and Engineering Foundation; the Polish State Committee for Scientific Research under contract No. 2P03B 17017; the Ministry of Science and Technology of the Russian Federation; the Ministry of Education, Science and Sport of the Republic of Slovenia; the National Science Council and the Ministry of Education of Taiwan; and the U.S. Department of Energy.

---

\* on leave from Nova Gorica Polytechnic, Nova Gorica

- [1] A. Ali, E. Lunghi, C. Greub, and G. Hiller, Phys. Rev. **D66**, 034002 (2002).
- [2] T. Hurth, hep-ph/0212304, SLAC-PUB-9604 (2003).
- [3] A. Ali, hep-ph/0210183, CERN-TH/2002-284 (2002).
- [4] K. Abe *et al.* [Belle Collaboration], Phys. Rev. Lett. **88**, 021801 (2002).
- [5] B. Aubert *et al.* [BaBar Collaboration], hep-ex/0207082, SLAC-PUB-9323 (2002).
- [6] A. Ishikawa *et al.* [Belle Collaboration], Phys. Rev. Lett. **91**, 261601 (2003).
- [7] B. Aubert *et al.* [BaBar Collaboration], Phys. Rev. Lett. **91**, 221802 (2003) [arXiv:hep-ex/0308042].
- [8] J. Kaneko *et al.* [Belle Collaboration], Phys. Rev. Lett. **90**, 021801 (2003).
- [9] B. Aubert *et al.* [BaBar Collaboration], arXiv:hep-ex/0308016.
- [10] The semi-inclusive technique was introduced in the context of inclusive  $B \rightarrow X_s \gamma$  decays; see M. S. Alam *et al.* [CLEO Collaboration], Phys. Rev. Lett. **74**, 2885 (1995).
- [11] S. Kurokawa and E. Kikutani, Nucl. Instrum. and Meth. **A499**, 1 (2003).
- [12] A. Abashian *et al.* [Belle Collaboration], Nucl. Instrum. and Meth. **A479**, 117 (2002).
- [13] D. J. Lange, Nucl. Instrum. and Meth. **A462**, 152 (2001).
- [14] T. Sjöstrand, Computer Physics Commun. **82**, 74 (1994).
- [15] R. Brun *et al.*, GEANT 3 Manual, CERN Program Library Long Writeup W5013, 1994.
- [16] A. Ali, P. Ball, L.T. Handoki, and G. Hiller, Phys. Rev. **D61**, 074024 (2000).
- [17] F. Krüger and L.M. Sehgal, Phys. Lett. **B380**, 199 (1996).
- [18] A. Ali and E. Pietarinen, Nucl. Phys. **B154**, 519 (1979); G. Altarelli *et al.*, Nucl. Phys. **B208**, 365 (1982).
- [19] R. A. Fisher, Annals Eugen. **7**, 179 (1936).
- [20] G.C. Fox and S. Wolfram, Phys. Rev. Lett. **41**, 1581 (1978).
- [21] H. Albrecht *et al.* [ARGUS Collaboration], Phys. Lett. **B192**, 245 (1987).
- [22] D. Cronin-Hennessy *et al.* [CLEO Collaboration], Phys. Rev. Lett. **87**, 251808 (2001).
- [23] S. Chen *et al.* [CLEO Collaboration], Phys. Rev. Lett. **87**, 251807 (2001).